Secondary organic aerosol formation from the OH-initiated oxidation of guaiacol under different experimental conditions

Changgeng Liu[a,b,1], Jun Liu[a,e,1], Yongchun Liu[c,*], Tianzeng Chen[a,e], Hong He[a,d,e,**]

[a] State Key Joint Laboratory of Environment Simulation and Pollution Control, Research Center for Eco-Environmental Sciences, Chinese Academy of Sciences, Beijing 100085, China
[b] School of Biological and Chemical Engineering, Panzhihua University, Panzhihua 617000, China
[c] Beijing Advanced Innovation Center for Soft Matter Science and Engineering, Beijing University of Chemical Technology, Beijing 100029, China
[d] Center for Excellence in Regional Atmospheric Environment, Institute of Urban Environment, Chinese Academy of Sciences, Xiamen 361021, China
[e] University of Chinese Academy of Sciences, Beijing 100049, China

GRAPHICAL ABSTRACT
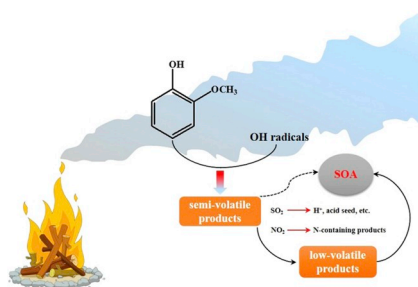
ARTICLE INFO

ABSTRACT

Guaiacol (2-methoxyphenol) has a high emission rate from wood burning and mainly exists in the gas phase, but the formation potential of secondary organic aerosol (SOA) from the atmospheric oxidation of guaiacol has not been well determined yet. In this work, SOA formation from the gas-phase reaction of guaiacol with OH radicals was investigated using an oxidation flow reactor (OFR) under different experimental conditions. The results showed that SOA yield was dependent on guaiacol concentration, OH exposure, and the presence of SO_2 and NO_2. SOA yield firstly increased and then decreased as a function of OH exposure. The maximum SOA yield (0.28–0.54) obtained at different guaiacol concentrations could be well-expressed by a one-product model. The SOA oxidation degree was represented by the carbon oxidation state (OS_C) and f_{44}/f_{43} (the ratio of organic mass fractions of m/z 44 to m/z 43), which both increased linearly and significantly with the increase of OH exposure. In addition, SO_2 and NO_2 promoted SOA formation, for which the maximum yield enhancements were 13.38% and 10.69%, respectively. The N/C ratio (0.034–0.045) indicated that NO_2 participated in the OH-initiated reaction of guaiacol, consequently resulting in the formation of organic nitrates. The experimental results would

* Corresponding author. Beijing Advanced Innovation Center for Soft Matter Science and Engineering, Beijing University of Chemical Technology, Beijing 100029, China.
** Corresponding author. State Key Joint Laboratory of Environment Simulation and Pollution Control, Research Center for Eco-Environmental Sciences, Chinese Academy of Sciences, Beijing 100085, China.
E-mail addresses: liuyc@buct.edu.cn (Y. Liu), honghe@rcees.ac.cn (H. He).
[1] These authors contributed equally to this work and should be considered as co-first authors.

be helpful to further the understanding of SOA formation from the atmospheric oxidation of guaiacol and its subsequent impacts on air quality and climate.

1. Introduction

Methoxyphenols are an important component of smoke emissions from biomass combustion, including natural fires, residential wood burning, and anthropogenic vegetation burning (Schauer et al., 2001; Simpson et al., 2005; Coeur-Tourneur et al., 2010a; Lauraguais et al., 2016). They are mainly derived from the pyrolysis of lignin, and are composed of guaiacol (2-methoxyphenol), syringol (2,6-dimethoxyphenol), and their derivatives (Nolte et al., 2001; Schauer et al., 2001; Simpson et al., 2005). Methoxyphenols are taken as potential tracers for wood smoke emissions due to their relatively high concentration in the atmosphere (Hawthorne et al., 1989, 1992; Simoneit et al., 1993). The total emission rate of methoxyphenols ranges from 900 to 4200 mg kg^{-1} wood (Hawthorne et al., 1989; Schauer et al., 2001; Simpson et al., 2005), and the total concentration in the atmosphere could reach several microgram per cubic meter (Hawthorne et al., 1992; Schauer and Cass, 2000; Simpson et al., 2005; Bari et al., 2009). In recent years, biomass-burning emissions have been reported to have a high secondary organic aerosol (SOA) formation potential via atmospheric oxidation (Bruns et al., 2016; Gilardoni et al., 2016; Ciarelli et al., 2017; Ding et al., 2017; Li et al., 2017), but SOA formation and growth from methoxyphenols are still poorly understood. Besides, the observed SOA levels in the atmosphere cannot be well explained by the present knowledge on SOA formation, indicating that a large number of precursors are not taken into account in the SOA-forming reactions included in the atmospheric models (Lauraguais et al., 2012).

2-Methoxyphenol (guaiacol) is a representative type of methoxyphenols widely detected in the gas-phase in the atmosphere, and has a high emission rate from fireplace combustion of wood (172–279 mg kg^{-1} wood) (Schauer et al., 2001). Its average emission concentration and factor from pine burning are 0.109 μg m^{-3} and 0.965 μg g^{-1} particle matter, respectively (Bari et al., 2009). The presence of guaiacol in urine could be used as a biomarker for its exposure (Bieniek and Stepien, 2011). Recently, the rate constants of homogeneous reactions of guaiacol with hydroxyl (OH) radicals (Coeur-Tourneur et al., 2010a), nitrate (NO$_3$) radicals (Lauraguais et al., 2016; Yang et al., 2016), chlorine atoms (Lauraguais et al., 2014a), and ozone (O$_3$) (El Zein et al., 2015) have been determined, indicating that its atmospheric degradation by OH and NO$_3$ radicals might be the predominant sink of guaiacol. Significant SOA formation from guaiacol via aqueous-phase reaction and photooxidation has been reported (Sun et al., 2010; Ofner et al., 2011). In addition, significant SOA formation from guaiacol with respect to its gas-phase reaction with OH radicals has been indicated (Yee et al., 2013; Lauraguais et al., 2014b; Ahmad et al., 2017). However, these works concentrated on the physicochemical properties of SOA (e.g., light absorption and hydrophilicity), SOA yield, oxidation products, and reaction mechanisms. To the best of our knowledge, the influences of OH exposure and precursor concentration on the chemical characteristics of SOA from the OH-initiated reaction of guaiacol have not yet been well elucidated. In addition, the possible impacts of SO$_2$ and NO$_2$ on SOA formation from guaiacol oxidation have not been investigated, even though their concentrations are up to 200 ppbv in the severely polluted atmospheres in China. Recently, it has been indicated that secondary formation of sulfate and SOA from biomass burning could significantly contribute to severe haze pollution (Li et al., 2017). For this reason, the aims of this work were to explore the effects of precursor concentration, OH exposure, SO$_2$, and NO$_2$ on SOA formation from the gas-phase reaction between guaiacol and OH radicals, using an oxidation flow reactor (OFR) at the relative humidity (RH) and temperature of (44.0 ± 2.0) % and (301 ± 1) K,

respectively.

2. Experimental section

The detailed schematic descriptions of the experimental system used in this work are shown in Figs. S1 and S2. The gas-phase reactions were conducted in the OFR, which has been described in detail elsewhere (Liu et al., 2014a,b). Before being introduced into the OFR, gas-phase species were mixed thoroughly in a mixing tube. The residence time in the OFR was 26.7 s, calculated on the basis of the illuminated volume (0.89 L) and the total flow rate (2 L min^{-1}). OH radicals were generated by the photolysis of O$_3$ in the presence of water vapor using a 254 nm UV lamp (Jelight Co. Inc.). The formation reactions were as follows: O$_3$ + $h\nu$ → O$_2$ + O(^{1}D) (λ = 254 nm) and O(^{1}D) + H$_2$O → 2·OH (Zhang et al., 2017). The concentration of OH radicals was governed by the O$_3$ concentration and RH, and the O$_3$ concentration was controlled by changing the shading length of a 185 nm UV lamp. O$_3$ was produced by passing zero air through an O$_3$ generator (model 610-220, Jelight Co. Inc.), and its concentration was in the range of 0.89–9.11 ppmv in this work, measured with an O$_3$ analyzer (model 205, 2B Technology Inc.). RH and temperature in the OFR were (44.0 ± 2.0) % and (301 ± 1) K, respectively, measured at the outlet of the OFR. The steady-state concentrations of OH radicals were determined using SO$_2$ as the reference compound in the separate calibration experiments (Zhang et al., 2017), and confirmed with a box model (Berresheim et al., 2003). This method is widely used for calculating OH exposure in the OFR, but could not well describe the potential suppression of OH exposure caused by the external OH reactivity (Lambe et al., 2015; Li et al., 2015; Peng et al., 2015, 2016; Simonen et al., 2017; Zhang et al., 2017). Although OH suppression by guaiacol was not well determined in the OFR, OH radicals were expected to be the main oxidant due to the fast reaction rate constant (7.53 × 10^{-11} cm^3 molecule^{-1} s^{-1}) of guaiacol toward OH radicals (Coeur-Tourneur et al., 2010a). The rate constant for the OH-initiated reaction of SO$_2$ is 9 × 10^{-13} cm^3 molecule^{-1} s^{-1} (Davis et al., 1979). The decay of SO$_2$ by OH radicals was measured by a SO$_2$ analyzer (model 43i, Thermo Fisher Scientific Inc.), and the corresponding concentration of OH radicals ([OH]) in this work ranged from approximately 3.8 × 10^9 to 4.7 × 10^{10} molecules cm^{-3}, with corresponding OH exposures in the range of 1.01–12.55 × 10^{11} molecules cm^{-3} s or approximately 0.78–9.68 days of equivalent atmospheric exposure.

In order to investigate the possible photolysis of guaiacol by 254 nm UV light in the OFR, the experiments were conducted with the UV lamp turned on and turned off. The results showed that no significant decay (< 5%) due to photolysis was observed and could be ignored. Based on the results reported by Peng et al. (2016), the photolysis of phenol compounds could be ignored when the ratio of exposure to 254 nm and OH radicals is lower than 1 × 10^6 cm s^{-1}, the values of which in this work also met this condition. In addition, the initial concentration of guaiacol was determined with the UV lamp turned on. Therefore, the effect of photolysis could be neglected in this work.

An Aerodyne high-resolution time-of-flight aerosol mass spectrometer (HR-ToF-AMS) was applied to online measure the chemical composition of particles and the non-refractory submicron aerosol mass (DeCarlo et al., 2006), and its signal at m/z 44 was corrected for interference from gas-phase CO$_2$ using a particle-free filter (Grieshop et al., 2007). The size distribution and concentration of particles were monitored by a scanning mobility particle sizer (SMPS), which is composed of a differential mobility analyzer (DMA) (model 3082, TSI Inc.) and a condensation particle counter (CPC) (model 3776, TSI Inc.).

Assuming that particles are spherical and non-porous, the average effective particle density could be calculated to be 1.5 g cm^{-3} using the equation $\rho = d_{va}/d_m$ (DeCarlo et al., 2004), where d_{va} is the mean vacuum aerodynamic diameter measured by HR-ToF-AMS and d_m is the mean volume-weighted mobility diameter measured by SMPS. The mass concentration of particles measured by HR-ToF-AMS was corrected by SMPS data in this work using the same method as Gordon et al. (2014). Gas-phase guaiacol was measured using a high-resolution proton-transfer-reaction time-of-flight mass spectrometer (HR-ToF-PTRMS) (Ionicon Analytik GmbH), and its concentration was calibrated by a commercial permeation tube (VICI AG International Valco Instruments Co., Inc.). Additional experimental details are described in the Supplementary data.

3. Results and discussion

3.1. Effects of precursor concentration and OH exposure on SOA formation

In order to explore the effects of guaiacol concentration and OH exposure on SOA formation from the OH-initiated reaction of guaiacol, a series of experiments were conducted at different guaiacol concentrations and OH exposures. The corresponding experimental conditions and maximum SOA yields are listed in Table 1. SOA yield was calculated as the ratio of SOA mass concentration (M_o, µg m^{-3}) to the consumed guaiacol concentration (Δ[guaiacol], µg m^{-3}) (Kang et al., 2007). The wall loss of aerosol particles in the OFR could be ignored, according to our previous results reported by Liu et al. (2014a,b). The changes of SOA yield versus OH exposure at different guaiacol concentrations are shown in Fig. S3. The results indicated that SOA yield was significantly dependent on both guaiacol concentration and OH exposure. In all cases, higher precursor concentrations resulted in higher amounts of condensable products and then enhanced SOA yield (Lauraguais et al., 2012). In previous studies, similar phenomena involving SOA formation from the oxidation of volatile organic compounds (VOCs) by OH radicals were observed in the smog chamber and Potential Aerosol Mass (PAM) reactor (Kang et al., 2007; Lauraguais et al., 2012, 2014b; Bruns et al., 2015; Lambe et al., 2015). In general, the SOA mass directly influences the gas-particle partitioning, because SOA could play the role of an adsorption medium of oxidation products; thus higher SOA mass generally leads to higher SOA yield (Lauraguais et al., 2012, 2014b). As illustrated in Fig. S3, SOA yield firstly increased and then decreased as a function of OH exposure, which is the most common trend in the PAM reactor and OFR (Kang et al., 2007; Bruns et al., 2015; Lambe et al., 2015). The possible explanation for this phenomenon might be ascribed to the C–C bond scission of gas-phase species by further oxidation or heterogeneous reactions involving OH radicals, consequently resulting in a large amount of fragmented molecules that could not condense on aerosol particles (Lambe et al., 2015;
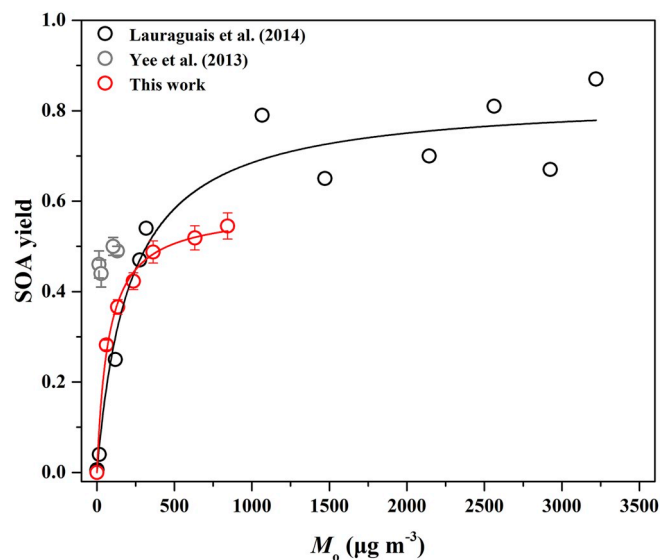

Fig. 1. SOA yield as a function of SOA mass concentration (M_o) formed from OH reactions at different guaiacol concentrations. The solid lines were fit to the experimental data using a one-product model. Values of α_i and $K_{om,i}$ used to generate the red line are (0.58 ± 0.02) and (0.014 ± 0.001) in this work, and their values are (0.83 ± 0.04) and (0.005 ± 0.001) for the black data from Lauraguais et al. (2014b). The gray data were obtained from Yee et al. (2013). (For interpretation of the references to colour in this figure legend, the reader is referred to the Web version of this article.)

Ortega et al., 2016; Simonen et al., 2017).

SOA yield could be represented by a semi-empirical model based on the absorptive gas-particle partitioning of semi-volatile products. The overall SOA yield (Y) is typically given by the following equation (Odum et al., 1996):

$$Y = \sum_i M_o \frac{\alpha_i K_{om,i}}{1 + K_{om,i} M_o} \tag{1}$$

where α_i is the mass-based stoichiometric coefficient for the reaction producing semi-volatile product i, $K_{om,i}$ is the gas-particle partitioning equilibrium constant, and M_o is the total aerosol mass concentration.

Fig. 1 shows the yield curve for guaiacol, obtained by plotting the SOA yield data in Table 1 according to Eq. (1). The experimental data could be accurately reproduced by a one-product model ($R^2 = 0.98$), while two or more products used in the model did not significantly improve the fitting quality. The obtained values of α_i and $K_{om,i}$ for the one-product model were (0.58 ± 0.02) and (0.014 ± 0.001) m^3 µg^{-1}, respectively. Odum et al. (1996) have indicated that SOA yields from the oxidation of aromatics could be described well by a two-product

Table 1
Experimental conditions and results in the absence of SO$_2$ and NO$_2$.

Exp.	[guaiacol]$_0$[a] (µg m^{-3})	$\triangle$[guaiacol][b] (µg m^{-3})	M_o[c] (µg m^{-3})	Y_{max}[d]	OH exposure[e] (10^{11} molecules cm^{-3} s)	τ[f] (days)
1	222	218	62	0.28	5.38	4.15
2	371	362	134	0.37	5.38	4.15
3	560	553	235	0.42	7.15	5.52
4	752	734	363	0.49	7.15	5.52
5	1224	1208	633	0.52	10.85	8.38
6	1553	1545	844	0.54	10.85	8.38

[a] Initial guaiacol concentrations.
[b] Reacted guaiacol concentrations.
[c] SOA mass concentrations.
[d] Maximum SOA yields.
[e] Corresponding OH exposures of maximum SOA yields.
[f] Corresponding atmospheric exposure time of maximum SOA yields, calculated using a typical [OH] in the atmosphere in this work (1.5 × 10^6 molecules cm^{-3}) (Mao et al., 2009).

model. Nevertheless, the one-product model has also been widely applied to describe SOA yields from the oxidation of aromatic compounds, including methoxyphenols (Coeur-Tourneur et al., 2010b; Lauraguais et al., 2012, 2014b). The simulation using the one-product model in this work is likely to indicate that the obtained α_i and $K_{om,i}$ are the average values for SOA. Since the composition of SOA was not determined, the volatility basis set (VBS) approach was not applied to simulate SOA yields. The plot shown in Fig. S4 is the relationship between the SOA mass concentration (M_o) and the reacted guaiacol concentration ($\triangle$[guaiacol]), the slope of which (0.60) is very close to the value of α_i (0.58). This suggested that the formed low-volatility products almost completely partitioned into the particle-phase according to the theoretical partition model (Lauraguais et al., 2012, 2014b). Considering the residence time in this work, there is a seeming contradiction with the recommendation of longer residence time made by Ahlberg et al. (2017), who reported that the condensation of low-volatility species on SOA in the OFR was often kinetically limited at low mass concentrations. Nevertheless, SOA yields obtained in this work could be comparable to those obtained in the chamber studies (Fig. 1). This suggests that the effect of kinetic limitations on SOA condensation for the OH-initiated oxidation of guaiacol in this system might be not important.

As shown in Fig. 1, SOA yields obtained in this work are slightly lower than those obtained in the smog chamber, which is similar to the results reported by Bruns et al. (2015). A possible explanation might be the increased wall losses of gas-phase species due to higher ratio of surface area to volume in the OFR, even when offset by better isolation of the sampled flow from the walls (Bruns et al., 2015). In previous work, SOA yields for guaiacol and syringol in gas-phase reactions with OH radicals have been determined in a smog chamber under high NO_2 concentrations (Lauraguais et al., 2012, 2014b). The maximum SOA yield of guaiacol (0.87) is much higher than that of syringol (0.36). Yee et al. (2013) also found that SOA yields of syringol (0.25–0.37) from the OH-initiated reaction were lower than those of guaiacol (0.44–0.50) under low-NO_x conditions with ammonium sulfate ((NH_4)$_2SO_4$) as seed particles. In addition, they also indicated that high NO concentration had an adverse impact on SOA formation (Yee et al., 2013). Under weakly acidic condition (pH = 5), Sun et al. (2010) found that the SOA mass formed from the aqueous-phase photochemical reaction of guaiacol in the presence of H_2O_2 was about twice as high as that in the absence of H_2O_2.

3.2. Oxidation state of SOA

The average carbon oxidation state (OS_C = 2O/C – H/C) is widely used to represent the oxidation degree of atmospheric OA, because it takes into account the saturation level of carbon atoms in the OA (Kroll et al., 2011). In addition, the organic mass fractions of m/z 44 (CO_2^+) and m/z 43 (mostly $C_2H_3O^+$), named f_{44} and f_{43}, respectively, are also used as indexes of the oxidation state of SOA (Ng et al., 2010; Kang et al., 2011; Bruns et al., 2015). In this work, the oxidation state of SOA formed at low (371 $\mu g\,m^{-3}$) and high (1553 $\mu g\,m^{-3}$) concentrations of guaiacol were compared. As shown in Fig. 2, the values of OS_C and the ratio of f_{44} to f_{43} (f_{44}/f_{43}) for the low concentration were much higher than those for the high concentration, suggesting that the formed SOA was more oxidized. This phenomenon was well supported by the evolution of SOA mass spectra (Fig. S5), f_{44}, and f_{43} (Fig. S6) obtained by HR-ToF-AMS at the same guaiacol concentrations. Similar phenomena have been observed in previous studies carried out in the smog chamber and PAM reactor (Loza et al., 2014; Ortega et al., 2016; Simonen et al., 2017). In addition, the results showed that OS_C and the f_{44}/f_{43} ratio increased linearly (R^2 > 0.98) and significantly when OH exposure increased from 1.01×10^{11} to 12.55×10^{11} molecules cm^{-3} s. In previous work, linear relationships between f_{44}/f_{43} ratio and OH exposure in the OH-initiated reactions of α-pinene, m-xylene, p-xylene, and their mixture were also observed (Kang et al., 2011).

In this work, the values of OS_C and f_{44} for SOA were up to 1.50 and

0.19, respectively, which are close to those for ambient low-volatility OA (LV-OA), and observed to be up to 1.9 (Kroll et al., 2011) and 0.25 (Ng et al., 2010). Recently, Ortega et al. (2016) also reported that the OS_C value for SOA formed from ambient air in the OFR could reach 2.0. In addition, the f_{44}/f_{43} ratio for SOA formed at low guaiacol concentration increased from 3.16 to 6.97, which is comparable to those for LV-OA observed in the atmosphere (Ng et al., 2010), even though the SOA mass concentrations in this work are much higher than those detected in the atmosphere. The higher values of OS_C and f_{44}/f_{43} ratio indicate the more aging state of the SOA, where the SOA components are further oxidized through heterogeneous oxidation, adding substantial oxygen and removing hydrogen from the molecules in the particle-phase to increase the oxidation state despite the overall loss of SOA mass (Ortega et al., 2016).

Positive matrix factorization (PMF) analysis of the HR-ToF-AMS data was applied to compare the chemical properties of SOA formed at three different guaiacol concentrations. Two factors were obtained from the PMF analysis, and their mass spectra are shown in Fig. S7. The values of f_{44} and f_{43} for Factor 1 were 0.12 and 0.028, respectively, higher than those (0.074 and 0.019) for Factor 2. Therefore, Factor 1 was tentatively assigned to the more-oxidized SOA, while Factor 2 was the less-oxidized SOA (Ulbrich et al., 2009). During the reaction process, these two factors had different change trends as a function of OH exposure. As shown in Fig. 3, Factor 1 always increased as OH exposure raised, while Factor 2 had an adverse trend. It should be noted that Factor 1 under low guaiacol concentration had a slight decrease at high OH exposure. The possible explanation might be that C–C bond scission of gas-phase species by further oxidation or heterogeneous reactions involving OH radicals produced more fragmented compounds, and a part of them could partition into aerosol particles (Lambe et al., 2015; Ortega et al., 2016; Simonen et al., 2017). At low OH exposure, the mass fractions of Factor 2 for all concentrations were relatively high, while increasing OH exposure was in favor of improving the mass fractions of Factor 1. A higher fraction of Factor 1 was obtained at low guaiacol concentration, suggesting that SOA formed at low guaiacol concentration mainly consisted of more-oxidized products with low volatility, which was well-supported by the changes of OS_C value and f_{44}/f_{43} ratio for SOA (Fig. 2). In addition, it should be noted that high guaiacol concentration resulted in relatively high SOA yield. The possible explanation might be that the increase of SOA mass concentration at high guaiacol concentration could be helpful to partition the less-oxidized products into the particle-phase once the initial nucleation was formed (Tröstl et al., 2016).
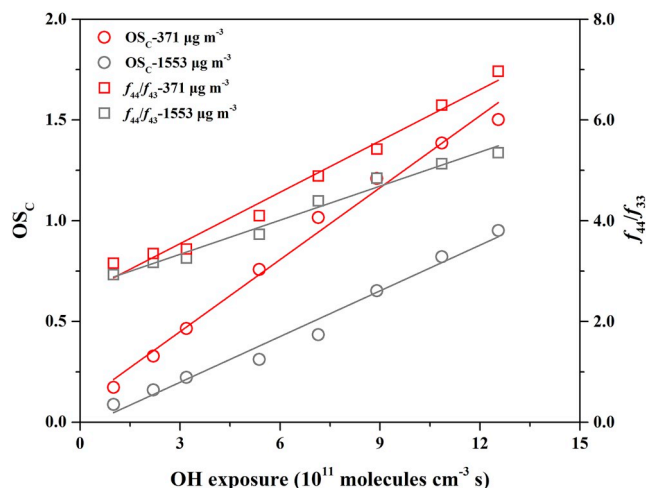

Fig. 2. OS_C and f_{44}/f_{43} ratio vs. OH exposure for SOA formed at two guaiacol concentrations (371 and 1553 $\mu g\,m^{-3}$).
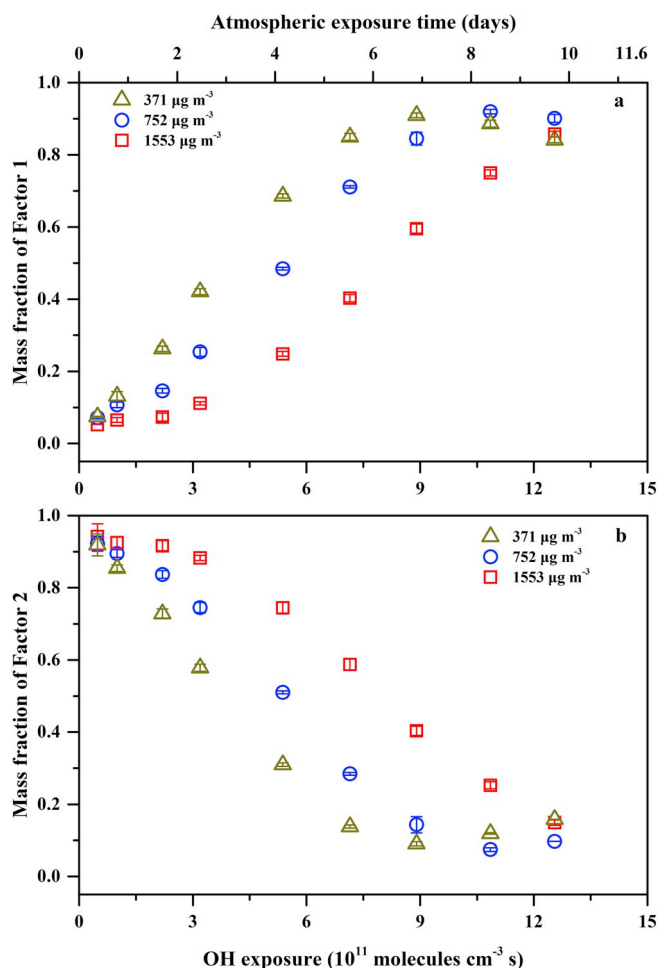
Fig. 3. Evolution of Factor 1 (a) and Factor 2 (b) as a function of OH exposure at three different guaiacol concentrations.
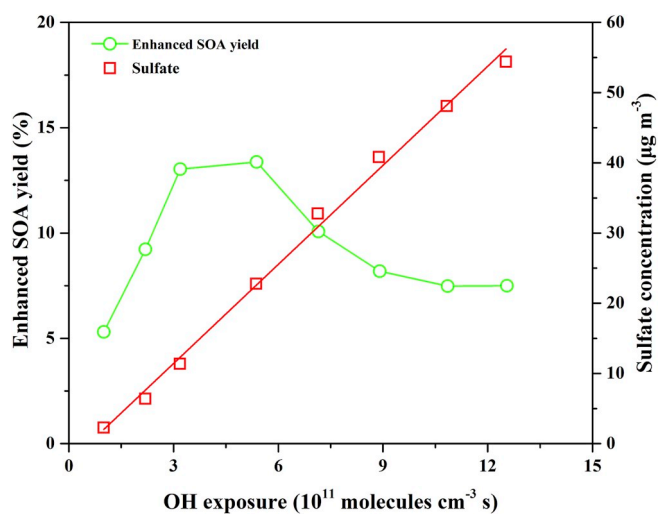

Fig. 4. Evolution of enhanced SOA yield and sulfate formation as a function of OH exposure in the presence of 60 ppbv SO_2 at the average guaiacol concentration of 368 μg m^{-3}.

3.3. Effect of SO_2 on SOA formation

As illustrated in Fig. 4, the presence of SO_2 promotes SOA formation. Additionally, the results showed that the sulfate concentration increased linearly ($R^2 = 0.99$) as a function of OH exposure. In the

presence of 60 ppbv SO_2, the maximum SOA yield enhancement of 13.38% was obtained at OH exposure of 5.38×10^{11} molecules cm^{-3} s, and then decreased with the increase of OH exposure, possibly due to the presence of fragmented molecules formed through gas-phase species oxidized by high OH exposure (Lambe et al., 2015; Ortega et al., 2016; Simonen et al., 2017). When the SO_2 concentration increased from 0 to 200 ppbv at OH exposure of 1.01×10^{11} molecules cm^{-3} s (Fig. S8), SOA yield (0.067–0.095) and sulfate concentration (0–10.90 μg m^{-3}) both increased linearly ($R^2 > 0.92$). In previous studies, Kleindienst et al. (2006) reported that SOA yield from α-pinene photooxidation increased by 40% in the presence of 252 ppbv SO_2; Liu et al. (2016b) recently found that SOA yield from the 5 h photochemical aging of gasoline vehicle exhaust was enhanced by (60–200) % in the presence of ~150 ppbv SO_2.

The results also showed that SO_2 had a significant impact on the size distribution of SOA particles. As shown in Fig. S9a, the mean diameter and number concentration of SOA particles in the absence of SO_2 were 26.29 nm and 9.37×10^6 cm^{-3}, respectively, increasing to 41.52 nm and 1.14×10^7 cm^{-3} in the presence of 60 ppbv SO_2 at OH exposure of 5.38×10^{11} molecules cm^{-3} s (Fig. S9b). As illustrated in Figs. 4 and S8, increasing sulfate concentration had a positive impact on SOA formation. In this system, it is difficult to completely remove trace NH_3, thus the formed sulfate was a mixture of sulfuric acid (H_2SO_4) and a small amount of $(NH_4)_2SO_4$. Based on the AIM-II model for the $H-NH_4^+ - SO_4^{2-} - NO_3^- - H_2O$ system (http://www.aim.env.uea.ac.uk/aim/model2/model2a.php; Liu et al., 2016b), the in situ particle acidity was calculated as the H^+ concentration ($[H^+]$, 28.98–690.59 nmol m^{-3}), the detailed calculation of which has been presented elsewhere (Liu et al., 2016b). The enhanced SOA yield was ascribed to the increased concentration of sulfuric acid in the particle-phase as the SO_2 concentration and OH exposure rose (Kleindienst et al., 2006; Liu et al., 2016b). In previous work, SOA yields from the oxidation of toluene and 1,3,5-trimethylbenzene increased by (14–36) % in the presence of acid seeds with $[H^+]$ of 240–860 nmol m^{-3} compared to those in the presence of nonacid seeds (Cao and Jang, 2007). Similar effects of particle acidity on SOA formation were also reported in other studies (Kleindienst et al., 2006; Jaoui et al., 2008; Liu et al., 2016b; Xu et al., 2016). Under acidic conditions, the gas-phase oxidation products partitioned into the particle-phase would be further oxidized into low-volatility products or produce oligomers via acid-catalyzed heterogeneous reactions, consequently enhancing SOA yields (Cao and Jang, 2007; Jaoui et al., 2008; Liu et al., 2016b; Xu et al., 2016). In addition, the formed H_2SO_4 not only serves as the substrate for product condensation and likely participates in the new particle formation (NPF) (Jaoui et al., 2008; Wang et al., 2016), but also enhances the surface areas of particles to facilitate the heterogeneous reactions on aerosols (Xu et al., 2016). These roles of H_2SO_4 also help to increase SOA yields. Recently, Friedman et al. (2016) indicated that SO_2 could participate in the oxidation reactions of pinene and perturbs its oxidation in the OFR, but this possible effect could be ignored in this work due to the relatively high RH and the negligible S/C ratio observed by HR-ToF-AMS (Friedman et al., 2016).

3.4. Effect of NO_2 on SOA formation

In general, high NO concentration always has an adverse impact on the formation of NPF and SOA, because of the reaction of NO with RO_2 radicals leading to the formation of more-volatile products compared to the reaction of HO_2 with RO_2 radicals (Sarrafzadeh et al., 2016). Previous studies reported that nitro-substituted products were the main products for SOA formed from OH-initiated reactions of phenol precursors, including methoxyphenols in the presence of NO_x (Lauraguais et al., 2012, 2014b; Ahmad et al., 2017; Finewax et al., 2018). Thus, the effect of NO_2 on SOA formation from guaiacol oxidation by OH radicals was investigated. As shown in Fig. 5, the presence of NO_2 was in favor of increasing SOA yield, but the nitrate concentration measured by HR-
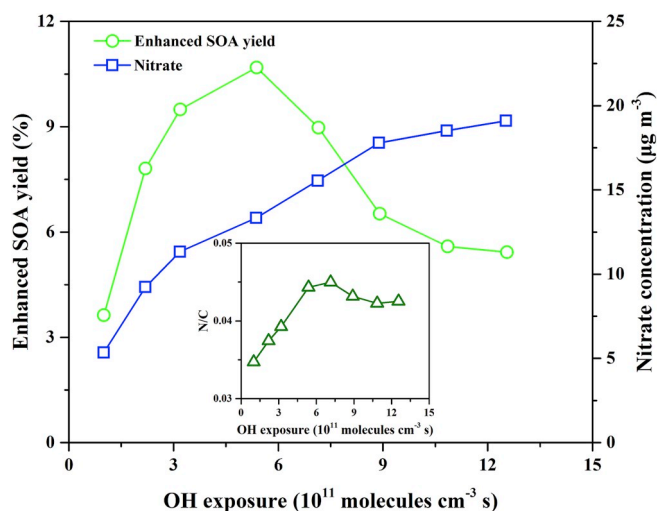
Fig. 5. Evolution of enhanced SOA yield, nitrate formation, and N/C ratio as a function of OH exposure in the presence of 60 ppbv NO_2 at the average guaiacol concentration of $368 \, \mu g \, m^{-3}$.

ToF-AMS was lower than the sulfate concentration, even if the OH rate constant of NO_2 is faster than that of SO_2 (Atkinson et al., 1976; Davis et al., 1979). The possible explanation might be that the formed HNO_3 mainly exists in the gas-phase and the relatively high temperature (301 ± 1 K) is not helpful for gaseous HNO_3 to distribute in the particle-phase (Wang et al., 2016). It has been reported that the temperature range for the greatest loss of nitrate is 293–298 K (Keck and Wittmaack, 2005). As shown in Fig. S9, the presence of NO_2 was also favorable for increasing the mean diameter and number concentration of SOA particles. The results also showed that the enhanced SOA yield and N/C ratio both increased firstly and then decreased with rising OH exposure. In addition, increasing the NO_2 concentration from 40 to 109 ppbv is slightly beneficial to SOA formation, N/C ratio, and nitrate formation, as shown in Fig. S10. Compared to the presence of 60 ppbv SO_2, the maximum enhancement of SOA yield (10.69%) in the presence of 60 ppbv NO_2 is lower. For most aromatic precursors, the addition of ppbv levels of NO_2 should have a negligible impact on SOA formation, because the rate constants of phenoxy radicals with O_2 and NO_2 are on the order of approximately 10^{-16} and 10^{-11} cm^3 molecule^{-1} s^{-1}, respectively (Atkinson and Arey, 2003). However, for phenol precursors, only about 0.5 ppbv NO_2 is sufficient to compete with O_2 for reaction with phenoxy radicals (Finewax et al., 2018). Therefore, the enhancement effect of NO_2 on SOA formation might be relevant to the special case of phenols but not for other aromatic precursors.

In this work, the N/C ratio was determined to be in the range of 0.034–0.045, indicating that NO_2 was incorporated in the reaction of OH radicals with guaiacol. This is in good agreement with the previously reported results, which found that nitro-substituted products were the main products of the OH-initiated reaction of guaiacol in the presence of NO_2 (Lauraguais et al., 2014b; Ahmad et al., 2017). The N-containing products might be also formed through reactions involving with NO_3 radicals, which are possibly generated by the reaction between NO_2 and O_3 in this system (Atkinson, 1991). The relatively low volatility of these products could reasonably contribute to SOA formation (Duporté et al., 2016; Liu et al., 2016a). In addition, a higher NO_2/NO ratio is helpful to the formation of nitro-substituted products, which are potentially involved NPF and SOA growth (Pereira et al., 2015). Ng et al. (2007) also indicated that NO_x could favor SOA formation from the oxidation of sesquiterpenes, due to the formation of low-volatility organic nitrates and the isomerization of large alkoxy radicals, resulting in less-volatile products. Recently, Hunter et al. (2014) reported that the N/C ratios for SOA formed from the OH reactions of cyclic alkanes ranged from 0.031 to 0.064, higher than those

obtained in this work. The decrease in the N/C ratio at high OH exposure suggested that more-volatile products were generated through the oxidation of particle-phase species by OH radicals.

In general, the measured NO^+/NO_2^+ ratios could be used to identify inorganic and organic nitrates. In this work, the measured NO^+/NO_2^+ ratios for inorganic nitrates were in the range of 2.06–2.54, determined by HR-ToF-AMS using ammonium nitrate as the calibration sample. These ratios were in good agreement with the NO^+/NO_2^+ ratios (1.08–2.81) for inorganic nitrates reported previously (Farmer et al., 2010; Sato et al., 2010). However, the NO^+/NO_2^+ ratios for the oxidation of guaiacol in the presence of 60 ppbv NO_2 were 4.02–6.25, which were higher than those for inorganic nitrates and in good agreement with those for organic nitrates (3.82–5.84) from the photooxidation of aromatics (Sato et al., 2010). The relative abundance of organic nitrates could be estimated from the N/C ratios determined in this work. Assuming that the oxidation products in the SOA retain seven carbon atoms, the yields of organic nitrates are in the range of (23.8–31.5) %, which are comparable to those reported in the earlier studies (Hunter et al., 2014; Liu et al., 2015). However, it should be noted that this range is the upper limit due to the possible C−C bond scission of gas- and particle-phase organics oxidized by high OH exposure.

3.5. Atmospheric implications

Recently, biomass burning was indicated to have great SOA formation potential through atmospheric oxidation (Bruns et al., 2016; Gilardoni et al., 2016; Ciarelli et al., 2017; Ding et al., 2017; Li et al., 2017). In addition, it is suggested that SOA formed from biomass burning plays an important role in haze pollution in China (Ding et al., 2017; Li et al., 2017). Methoxyphenols are one of the major components of biomass-burning smoke, and are emitted into the atmosphere with relatively high concentration (Schauer and Cass, 2000; Bruns et al., 2016). According to our results and the previous studies (Sun et al., 2010; Lauraguais et al., 2012, 2014b; Yee et al., 2013; Ahmad et al., 2017), the significant SOA formation potential from the oxidation of methoxyphenols by OH radicals and its subsequent effects on haze evolution should be paid more attention, especially in China with nationwide biomass burning and high daytime average [OH] in the ambient atmosphere ($(5.2–7.5) \times 10^6$ molecules cm^{-3}) (Yang et al., 2017). Although the guaiacol concentrations in this work are higher than its atmospheric levels (Nolte et al., 2001; Simpson et al., 2005; Bari et al., 2009), the results obtained in this work might be helpful for air quality simulation modeling of specific regions that are experiencing serious pollution resulting from biomass burning. In addition, it should be noted that the atmospheric exposure time has a significant impact on SOA formation. Longer atmospheric exposure time will decrease SOA formation, possibly because fragmentation might be more important than functionalization (Tkacik et al., 2014). Recently, Liu et al. (2018) reported that the greatest SOA formation from Beijing urban ambient air was achieved at the atmospheric exposure time of 2–4 days, depending on the concentrations of VOCs in the air. Therefore, in order to more accurately predict SOA formation from VOC oxidation, the atmospheric exposure time for VOC oxidation should be seriously taken into account.

The results obtained in this work might indicate that the OH-initiated reactions of methoxyphenols represent an important pathway for the formation of low-volatility and highly oxygenated organic species, subsequently affecting the optical absorption and hygroscopic properties of atmospheric particles (Massoli et al., 2010; Lambe et al., 2013). In addition, SO_2 and NO_2 were found to promote SOA formation from guaiacol oxidation, suggesting that the possibly synergetic contributions of SOA from biomass burning and the oxidation of SO_2 and NO_2 to haze pollution should be further understood, due to the high levels of SO_2 and NO_2 in the severely polluted atmospheres in China (Li et al., 2017). Therefore, SOA formed from the atmospheric oxidation of methoxyphenols might have important effects on air quality and

climate. Moreover, the experimental results could help to further the understanding of the atmospheric aging process of smoke plumes from biomass burning.

4. Conclusions

In this work, SOA formation from the OH-initiated reaction of guaiacol under different environmental conditions was investigated in the OFR. The results showed that SOA yield was dependent on guaiacol concentration, and firstly increased and then decreased as a function of OH exposure. The maximum SOA yield (0.28–0.54) obtained at different guaiacol concentrations could be expressed well by a one-product model. OS_C and f_{44}/f_{43} of SOA both increased linearly as a function of OH exposure. In addition, the presence of SO_2 and NO_2 was in favor of increasing SOA yield, and the maximum yield enhancements were 13.38% and 10.69%, respectively. The N/C ratio (0.034–0.045) suggested that NO_2 participated in the OH-initiated reaction of guaiacol, consequently resulting in the formation of organic nitrates. The experimental results might be helpful to further the understanding of SOA formation from the atmospheric oxidation of guaiacol by OH radicals.

Appendix A. Supplementary data

Supplementary data to this article can be found online at https://doi.org/10.1016/j.atmosenv.2019.03.021.

References

Ahlberg, E., Falk, J., Eriksson, A., Holst, T., Brune, W.H., Kristensson, A., Roldin, P., Svenningsson, B., 2017. Secondary organic aerosol from VOC mixtures in an oxidation flow reactor. Atmos. Environ. 161, 210–220.

Ahmad, W., Coeur, C., Tomas, A., Fagniez, T., Brubach, J.-B., Cuisset, A., 2017. Infrared spectroscopy of secondary organic aerosol precursors and investigation of the hygroscopicity of SOA formed from the OH reaction with guaiacol and syringol. Appl. Opt. 56, E116–E122.

Atkinson, R., 1991. Kinetics and mechanisms of the gas-phase reactions of the NO_3 radical with organic compounds. J. Phys. Chem. Ref. Data 20, 459–507.

Atkinson, R., Arey, J., 2003. Atmospheric degradation of volatile organic compounds. Chem. Rev. 103, 4605–4638.

Atkinson, R., Perry, R.A., Pitts, J.N., 1976. Rate constants for the reactions of the OH radicals with NO_2 (M = Ar and N_2) and SO_2 (M = Ar). J. Chem. Phys. 65, 306–310.

Bari, M.A., Baumbach, G., Kuch, B., Scheffknecht, G., 2009. Wood smoke as a source of particle-phase organic compounds in residential areas. Atmos. Environ. 43, 4722–4732.

Berresheim, H., Plass-Dülmer, C., Elste, T., Mihalopoulos, N., Rohrer, F., 2003. OH in the coastal boundary layer of Crete during MINOS: measurements and relationship with ozone photolysis. Atmos. Chem. Phys. 3, 639–649.

Bieniek, G., Stepien, K., 2011. Occupational exposure to phenolic compounds at coke plants-urinary excretion of methoxyphenols as an indicator of exposure to methoxyphenols. J. Occup. Health 53, 110–114.

Bruns, E.A., El Haddad, I., Keller, A., Klein, F., Kumar, N.K., Pieber, S.M., Corbin, J.C., Slowik, J.G., Brune, W.H., Baltensperger, U., Prevot, A.S.H., 2015. Inter-comparison of laboratory smog chamber and flow reactor systems on organic aerosol yield and composition. Atmos. Meas. Tech. 8, 2315–2332.

Bruns, E.A., El Haddad, I., Slowik, J.G., Kilic, D., Klein, F., Baltensperger, U., Prevot, A.S.H., 2016. Identification of significant precursor gases of secondary organic aerosols from residential wood combustion. Sci. Rep. 6, 27881. https://doi.org/10.1038/srep27881.

Cao, G., Jang, M., 2007. Effects of particle acidity and UV light on secondary organic aerosol formation from oxidation of aromatics in the absence of NO_x. Atmos. Environ. 41, 7603–7613.

Ciarelli, G., Aksoyoglu, S., El Haddad, I., Bruns, E.A., Crippa, M., Poulain, L., Aijala, M., Carbone, S., Freney, E., O'Dowd, C., Baltensperger, U., Prevot, A.S.H., 2017. Modelling winter organic aerosol at the European scale with CAMx: evaluation and source apportionment with a VBS parameterization based on novel wood burning smog chamber experiments. Atmos. Chem. Phys. 7, 7653–7669.

Coeur-Tourneur, C., Cassez, A., Wenger, J.C., 2010a. Rate coefficients for the gas-phase reaction of hydroxyl radicals with 2-methoxyphenol (guaiacol) and related compounds. J. Phys. Chem. A 114, 11645–11650.

Coeur-Tourneur, C., Foulon, V., Lareal, M., 2010b. Determination of aerosol yields from 3-methylcatechol and 4-methylcatechol ozonolysis in a simulation chamber. Atmos. Environ. 44, 852–857.

Davis, D.D., Ravishankara, A.R., Fischer, S., 1979. SO_2 oxidation via the hydroxyl radical: atmospheric fate of HSO_x radicals. Geophys. Res. Lett. 6, 113–116.

DeCarlo, P.F., Kimmel, J.R., Trimborn, A., Northway, M.J., Jayne, J.T., Aiken, A.C., Gonin, M., Fuhrer, K., Horvath, T., Docherty, K.S., Worsnop, D.R., Jimenez, J.L., 2006. Field-deployable, high-resolution, time-of-flight aerosol mass spectrometer. Anal. Chem. 78, 8281–8289.

DeCarlo, P.F., Slowik, J.G., Worsnop, D.R., Davidovits, P., Jimenez, J.L., 2004. Particle morphology and density characterization by combined mobility and aerodynamic diameter measurements. Part 1: theory. Aerosol Sci. Technol. 38, 1185–1205.

Ding, X., Zhang, Y.Q., He, Q.-F., Yu, Q.Q., Wang, J.Q., Shen, R.Q., Song, W., Wang, Y.S., Wang, X.M., 2017. Significant increase of aromatics-derived secondary organic aerosol during fall to winter in China. Environ. Sci. Technol. 51, 7432–7441.

Duporté, G., Parshintsev, J., Barreira, L.M.F., Hartonen, K., Kulmala, M., Riekkola, M.-L., 2016. Nitrogen-containing low volatile compounds from pinonaldehyde-dimethylamine reaction in the atmosphere: a laboratory and field study. Environ. Sci. Technol. 50, 4693–4700.

El Zein, A., Coeur, C., Obeid, E., Lauraguais, A., Fagniez, T., 2015. Reaction kinetics of catechol (1,2-benzenediol) and guaiacol (2-methoxyphenol) with ozone. J. Phys. Chem. A 119, 6759–6765.

Farmer, D.K., Matsunaga, A., Docherty, K.S., Surratt, J.D., Seinfeld, J.H., Ziemann, P.J., Jimenez, J.L., 2010. Response of an aerosol mass spectrometer to organonitrates and organosulfates and implications for atmospheric chemistry. Proc. Natl. Acad. Sci. U. S. A. 107, 6670–6675.

Finewax, Z., de Gouw, J.A., Ziemann, P.J., 2018. Identification and quantification of 4-nitrocatechol formed from OH and NO_3 radical-initiated reactions of catechol in air in the presence of NO_x: implications for secondary organic aerosol formation from biomass burning. Environ. Sci. Technol. 52, 1981–1989.

Friedman, B., Brophy, P., Brune, W.H., Farmer, D.K., 2016. Anthropogenic sulfur perturbations on biogenic oxidation: SO_2 additions impact gas-phase OH oxidation products of α- and β-pinene. Environ. Sci. Technol. 50, 1269–1279.

Gilardoni, S., Massoli, P., Paglione, M., Giulianelli, L., Carbone, C., Rinaldi, M., Decesari, S., Sandrini, S., Costabile, F., Gobbi, G.P., Pietrogrande, M.C., Visentin, M., Scotto, F., Fuzzi, S., Facchini, M.C., 2016. Direct observation of aqueous secondary organic aerosol from biomass-burning emissions. Proc. Natl. Acad. Sci. U. S. A. 113, 10013–10018.

Gordon, T.D., Presto, A.A., Nguyen, N.T., Robertson, W.H., Na, K., Sahay, K.N., Zhang, M., Maddox, C., Rieger, P., Chattopadhyay, S., Maldonado, H., Maricq, M.M., Robinson, A.L., 2014. Secondary organic aerosol production from diesel vehicle exhaust: impact of aftertreatment, fuel chemistry and driving cycle. Atmos. Chem. Phys. 14, 4643–4659.

Grieshop, A.P., Donahue, N.M., Robinson, A.L., 2007. Is the gas-particle partitioning in α-pinene secondary organic aerosol reversible? Geophys. Res. Lett. 34, L14810. https://doi.org/10.1029/2007GL029987.

Hawthorne, S.B., Krieger, M.S., Miller, D.J., Mathiason, M.B., 1989. Collection and quantitation of methoxylated phenol tracers for atmospheric pollution from residential wood stoves. Environ. Sci. Technol. 23, 470–475.

Hawthorne, S.B., Miller, D.J., Langenfeld, J.J., Krieger, M.S., 1992. PM_{10} high-volume collection and quantitation of semivolatile and nonvolatile phenols, methoxylated phenols, alkanes, and polycyclic aromatic hydrocarbons from winter urban air and their relationship to wood smoke emissions. Environ. Sci. Technol. 26, 2251–2262. http://www.aim.env.uea.ac.uk/aim/model2/model2a.php, Accessed date: 8 July 2018.

Hunter, J.F., Carrasquillo, A.J., Daumit, K.E., Kroll, J.H., 2014. Secondary organic aerosol formation from acyclic, monocyclic, and polycyclic alkanes. Environ. Sci. Technol. 48, 10227–10234.

Jaoui, M., Edney, E.O., Kleindienst, T.E., Lewandowski, M., Offenberg, J.H., Surratt, J.D., Seinfeld, J.H., 2008. Formation of secondary organic aerosol from irradiated α-pinene/toluene/NO_x mixtures and the effect of isoprene and sulfur dioxide. J. Geophys. Res. Atmos. 113, D09303. https://doi.org/10.1029/2007jd009426.

Kang, E., Root, M.J., Toohey, D.W., Brune, W.H., 2007. Introducing the concept of potential aerosol mass (PAM). Atmos. Chem. Phys. 7, 5727–5744.

Kang, E., Toohey, D.W., Brune, W.H., 2011. Dependence of SOA oxidation on organic aerosol mass concentration and OH exposure: experimental PAM chamber studies. Atmos. Chem. Phys. 11, 1837–1852.

Keck, L., Wittmaack, K., 2005. Effect of filter type and temperature on volatilisation losses from ammonium salts in aerosol matter. Atmos. Environ. 39, 4093–4100.

Kleindienst, T.E., Edney, E.O., Lewandowski, M., Offenberg, J.H., Jaoui, M., 2006. Secondary organic carbon and aerosol yields from the irradiations of isoprene and α-pinene in the presence of NO_x and SO_2. Environ. Sci. Technol. 40, 3807–3812.

Kroll, J.H., Donahue, N.M., Jimenez, J.L., Kessler, S.H., Canagaratna, M.R., Wilson, K.R., Altieri, K.E., Mazzoleni, L.R., Wozniak, A.S., Bluhm, H., Mysak, E.R., Smith, J.D., Kolb, C.E., Worsnop, D.R., 2011. Carbon oxidation state as a metric for describing the chemistry of atmospheric organic aerosol. Nat. Chem. 3, 133–139.

Lambe, A.T., Cappa, C.D., Massoli, P., Onasch, T.B., Forestieri, S.D., Martin, A.T., Cummings, M.J., Croasdale, D.R., Brune, W.H., Worsnop, D.R., Davidovits, P., 2013. Relationship between oxidation level and optical properties of secondary organic aerosol. Environ. Sci. Technol. 47, 6349–6357.

Lambe, A.T., Chhabra, P.S., Onasch, T.B., Brune, W.H., Hunter, J.F., Kroll, J.H., Cummings, M.J., Brogan, J.F., Parmar, Y., Worsnop, D.R., Kolb, C.E., Davidovits, P., 2015. Effect of oxidant concentration, exposure time, and seed particles on secondary organic aerosol chemical composition and yield. Atmos. Chem. Phys. 15, 3063–3075.

Lauraguais, A., Bejan, I., Barnes, I., Wiesen, P., Coeur-Tourneur, C., Cassez, A., 2014a. Rate coefficients for the gas-phase reaction of chlorine atoms with a series of methoxylated aromatic compounds. J. Phys. Chem. A 118, 1777–1784.

Lauraguais, A., Coeur-Tourneur, C., Cassez, A., Deboudt, K., Fourmentin, M., Choel, M., 2014b. Atmospheric reactivity of hydroxyl radicals with guaiacol (2-methoxyphenol), a biomass burning emitted compound: secondary organic aerosol formation and gas-phase oxidation products. Atmos. Environ. 86, 155–163.

Lauraguais, A., Coeur-Tourneur, C., Cassez, A., Seydi, A., 2012. Rate constant and secondary organic aerosol yields for the gas-phase reaction of hydroxyl radicals with syringol (2,6-dimethoxyphenol). Atmos. Environ. 55, 43–48.

Lauraguais, A., El Zein, A., Coeur, C., Obeid, E., Cassez, A., Rayez, M.-T., Rayez, J.-C., 2016. Kinetic study of the gas-phase reactions of nitrate radicals with methoxyphenol compounds: experimental and theoretical approaches. J. Phys. Chem. A 120, 2691–2699.

Li, H., Zhang, Q., Zhang, Q., Chen, C., Wang, L., Wei, Z., Zhou, S., Parworth, C., Zheng, B., Canonaco, F., Prevot, A.S.H., Chen, P., Zhang, H., Wallington, T.J., He, K., 2017. Wintertime aerosol chemistry and haze evolution in an extremely polluted city of the North China Plain: significant contribution from coal and biomass combustion. Atmos. Chem. Phys. 17, 4751–4768.

Li, R., Palm, B.B., Ortega, A.M., Hlywiak, J., Hu, W., Peng, Z., Day, D.A., Knote, C., Brune, W.H., de Gouw, J.A., Jimenez, J.L., 2015. Modeling the radical chemistry in an oxidation flow reactor: radical formation and recycling, sensitivities, and the OH exposure estimation equation. J. Phys. Chem. A 119, 4418–4432.

Liu, J., Chu, B., Chen, T., Liu, C., Wang, L., Bao, X., He, H., 2018. Secondary organic aerosol formation from ambient air at an urban site in beijing: effects of OH exposure and precursor concentrations. Environ. Sci. Technol. 52, 6834–6841.

Liu, J., Lin, P., Laskin, A., Laskin, J., Kathmann, S.M., Wise, M., Caylor, R., Imholt, F., Selimovic, V., Shilling, J.E., 2016a. Optical properties and aging of light-absorbing secondary organic aerosol. Atmos. Chem. Phys. 16, 12815–12827.

Liu, T., Wang, X., Hu, Q., Deng, W., Zhang, Y., Ding, X., Fu, X., Bernard, F., Zhang, Z., Lu, S., He, Q., Bi, X., Chen, J., Sun, Y., Yu, J., Peng, P., Sheng, G., Fu, J., 2016b. Formation of secondary aerosols from gasoline vehicle exhaust when mixing with SO_2. Atmos. Chem. Phys. 16, 675–689.

Liu, Y., Huang, L., Li, S.M., Harner, T., Liggio, J., 2014a. OH-initiated heterogeneous oxidation of tris-2-butoxyethyl phosphate: implications for its fate in the atmosphere. Atmos. Chem. Phys. 14, 12195–12207.

Liu, Y., Liggio, J., Harner, T., Jantunen, L., Shoeib, M., Li, S.-M., 2014b. Heterogeneous OH initiated oxidation: a possible explanation for the persistence of organophosphate flame retardants in air. Environ. Sci. Technol. 48, 1041–1048.

Liu, Y., Liggio, J., Staebler, R., Li, S.M., 2015. Reactive uptake of ammonia to secondary organic aerosols: kinetics of organonitrogen formation. Atmos. Chem. Phys. 15, 13569–13584.

Loza, C.L., Craven, J.S., Yee, L.D., Coggon, M.M., Schwantes, R.H., Shiraiwa, M., Zhang, X., Schilling, K.A., Ng, N.L., Canagaratna, M.R., Ziemann, P.J., Flagan, R.C., Seinfeld, J.H., 2014. Secondary organic aerosol yields of 12-carbon alkanes. Atmos. Chem. Phys. 14, 1423–1439.

Mao, J., Ren, X., Brune, W.H., Olson, J.R., Crawford, J.H., Fried, A., Huey, L.G., Cohen, R.C., Heikes, B., Singh, H.B., Blake, D.R., Sachse, G.W., Diskin, G.S., Hall, S.R., Shetter, R.E., 2009. Airborne measurement of OH reactivity during INTEX-B. Atmos. Chem. Phys. 9, 163–173.

Massoli, P., Lambe, A.T., Ahern, A.T., Williams, L.R., Ehn, M., Mikkila, J., Canagaratna, M.R., Brune, W.H., Onasch, T.B., Jayne, J.T., Petaja, T., Kulmala, M., Laaksonen, A., Kolb, C.E., Davidovits, P., Worsnop, D.R., 2010. Relationship between aerosol oxidation level and hygroscopic properties of laboratory generated secondary organic aerosol (SOA) particles. Geophys. Res. Lett. 37, L24801. https://doi.org/10.1029/2010gl045258.

Ng, N.L., Canagaratna, M.R., Zhang, Q., Jimenez, J.L., Tian, J., Ulbrich, I.M., Kroll, J.H., Docherty, K.S., Chhabra, P.S., Bahreini, R., Murphy, S.M., Seinfeld, J.H., Hildebrandt, L., Donahue, N.M., DeCarlo, P.F., Lanz, V.A., Prevot, A.S.H., Dinar, E., Rudich, Y., Worsnop, D.R., 2010. Organic aerosol components observed in northern hemispheric datasets from aerosol mass spectrometry. Atmos. Chem. Phys. 10, 4625–4641.

Ng, N.L., Chhabra, P.S., Chan, A.W.H., Surratt, J.D., Kroll, J.H., Kwan, A.J., McCabe, D.C., Wennberg, P.O., Sorooshian, A., Murphy, S.M., Dalleska, N.F., Flagan, R.C., Seinfeld, J.H., 2007. Effect of NO_x level on secondary organic aerosol (SOA) formation from the photooxidation of terpenes. Atmos. Chem. Phys. 7, 5159–5174.

Nolte, C.G., Schauer, J.J., Cass, G.R., Simoneit, B.R.T., 2001. Highly polar organic compounds present in wood smoke and in the ambient atmosphere. Environ. Sci. Technol. 35, 1912–1919.

Odum, J.R., Hoffmann, T., Bowman, F., Collins, D., Flagan, R.C., Seinfeld, J.H., 1996. Gas/particle partitioning and secondary organic aerosol yields. Environ. Sci. Technol. 30, 2580–2585.

Ofner, J., Krueger, H.U., Grothe, H., Schmitt-Kopplin, P., Whitmore, K., Zetzsch, C., 2011. Physico-chemical characterization of SOA derived from catechol and guaiacol - a model substance for the aromatic fraction of atmospheric HULIS. Atmos. Chem. Phys. 11, 1–15.

Ortega, A.M., Hayes, P.L., Peng, Z., Palm, B.B., Hu, W., Day, D.A., Li, R., Cubison, M.J., Brune, W.H., Graus, M., Warneke, C., Gilman, J.B., Kuster, W.C., de Gouw, J.,

Gutierrez-Montes, C., Jimenez, J.L., 2016. Real-time measurements of secondary organic aerosol formation and aging from ambient air in an oxidation flow reactor in the Los Angeles area. Atmos. Chem. Phys. 16, 7411–7433.

Peng, Z., Day, D.A., Ortega, A.M., Palm, B.B., Hu, W., Stark, H., Li, R., Tsigaridis, K., Brune, W.H., Jimenez, J.L., 2016. Non-OH chemistry in oxidation flow reactors for the study of atmospheric chemistry systematically examined by modeling. Atmos. Chem. Phys. 16, 4283–4305.

Peng, Z., Day, D.A., Stark, H., Li, R., Lee-Taylor, J., Palm, B.B., Brune, W.H., Jimenez, J.L., 2015. HO_x radical chemistry in oxidation flow reactors with low-pressure mercury lamps systematically examined by modeling. Atmos. Meas. Tech. 8, 4863–4890.

Pereira, K.L., Hamilton, J.F., Rickard, A.R., Bloss, W.J., Alam, M.S., Camredon, M., Ward, M.W., Wyche, K.P., Munoz, A., Vera, T., Vazquez, M., Borras, E., Rodenas, M., 2015. Insights into the formation and evolution of individual compounds in the particulate phase during aromatic photo-oxidation. Environ. Sci. Technol. 49, 13168–13178.

Sarrafzadeh, M., Wildt, J., Pullinen, I., Springer, M., Kleist, E., Tillmann, R., Schmitt, S.H., Wu, C., Mentel, T.F., Zhao, D., Hastie, D.R., Kiendler-Scharr, A., 2016. Impact of NO_x and OH on secondary organic aerosol formation from beta-pinene photooxidation. Atmos. Chem. Phys. 16, 11237–11248.

Sato, K., Takami, A., Isozaki, T., Hikida, T., Shimono, A., Imamura, T., 2010. Mass spectrometric study of secondary organic aerosol formed from the photo-oxidation of aromatic hydrocarbons. Atmos. Environ. 44, 1080–1087.

Schauer, J.J., Cass, G.R., 2000. Source apportionment of wintertime gas-phase and particle-phase air pollutants using organic compounds as tracers. Environ. Sci. Technol. 34, 1821–1832.

Schauer, J.J., Kleeman, M.J., Cass, G.R., Simoneit, B.R.T., 2001. Measurement of emissions from air pollution sources. 3. C-1-C-29 organic compounds from fireplace combustion of wood. Environ. Sci. Technol. 35, 1716–1728.

Simoneit, B.R.T., Rogge, W.F., Mazurek, M.A., Standley, L.J., Hildemann, L.M., Cass, G.R., 1993. Lignin pyrolysis products, lignans, and resin acid as specific tracers of plant classes in emissions from biomass combustion. Environ. Sci. Technol. 27, 2533–2541.

Simonen, P., Saukko, E., Karjalainen, P., Timonen, H., Bloss, M., Aakko-Saksa, P., Ronkko, T., Keskinen, J., Dal Maso, M., 2017. A new oxidation flow reactor for measuring secondary aerosol formation of rapidly changing emission sources. Atmos. Meas. Tech. 10, 1519–1537.

Simpson, C.D., Paulsen, M., Dills, R.L., Liu, L.J.S., Kalman, D.A., 2005. Determination of methoxyphenols in ambient atmospheric particulate matter: tracers for wood combustion. Environ. Sci. Technol. 39, 631–637.

Sun, Y.L., Zhang, Q., Anastasio, C., Sun, J., 2010. Insights into secondary organic aerosol formed via aqueous-phase reactions of phenolic compounds based on high resolution mass spectrometry. Atmos. Chem. Phys. 10, 4809–4822.

Tkacik, D.S., Lambe, A.T., Jathar, S., Li, X., Presto, A.A., Zhao, Y., Blake, D., Meinardi, S., Jayne, J.T., Croteau, P.L., Robinson, A.L., 2014. Secondary organic aerosol formation from in-use motor vehicle emissions using a Potential Aerosol Mass reactor. Environ. Sci. Technol. 48, 11235–11242.

Tröstl, J., Chuang, W.K., Gordon, H., Heinritzi, M., Yan, C., Molteni, U., Ahlm, L., Frege, C., Bianchi, F., Wagner, R., Simon, M., Lehtipalo, K., Williamson, C., Craven, J.S., Duplissy, J., Adamov, A., Almeida, J., Bernhammer, A.-K., Breitenlechner, M., Brilke, S., Dias, A., Ehrhart, S., Flagan, R.C., Franchin, A., Fuchs, C., Guida, R., Gysel, M., Hansel, A., Hoyle, C.R., Jokinen, T., Junninen, H., Kangasluoma, J., Keskinen, H., Kim, J., Krapf, M., Kürten, A., Laaksonen, A., Lawler, M., Leiminger, M., Mathot, S., Möhler, O., Nieminen, T., Onnela, A., Petäjä, T., Piel, F.M., Miettinen, P., Rissanen, M.P., Rondo, L., Sarnela, N., Schobesberger, S., Sengupta, K., Sipilä, M., Smith, J.N., Steiner, G., Tomè, A., Virtanen, A., Wagner, A.C., Weingartner, E., Wimmer, D., Winkler, P.M., Ye, P., Carslaw, K.S., Curtius, J., Dommen, J., Kirkby, J., Kulmala, M., Riipinen, I., Worsnop, D.R., Donahue, N.M., Baltensperger, U., 2016. The role of low-volatility organic compounds in initial particle growth in the atmosphere. Nature 533, 527.

Ulbrich, I.M., Canagaratna, M.R., Zhang, Q., Worsnop, D.R., Jimenez, J.L., 2009. Interpretation of organic components from Positive Matrix Factorization of aerosol mass spectrometric data. Atmos. Chem. Phys. 9, 2891–2918.

Wang, D., Zhou, B., Fu, Q., Zhao, Q., Zhang, Q., Chen, J., Yang, X., Duan, Y., Li, J., 2016. Intense secondary aerosol formation due to strong atmospheric photochemical reactions in summer: observations at a rural site in eastern Yangtze River Delta of China. Sci. Total Environ. 571, 1454–1466.

Xu, L., Middlebrook, A.M., Liao, J., de Gouw, J.A., Guo, H., Weber, R.J., Nenes, A., Lopez-Hilfiker, F.D., Lee, B.H., Thornton, J.A., Brock, C.A., Neuman, J.A., Nowak, J.B., Pollack, I.B., Welti, A., Graus, M., Warneke, C., Ng, N.L., 2016. Enhanced formation of isoprene-derived organic aerosol in sulfur-rich power plant plumes during Southeast Nexus. J. Geophys. Res. Atmos. 121, 11137–11153.

Yang, B., Zhang, H., Wang, Y., Zhang, P., Shu, J., Sun, W., Ma, P., 2016. Experimental and theoretical studies on gas-phase reactions of NO_3 radicals with three methoxyphenols: guaiacol, creosol, and syringol. Atmos. Environ. 125, 243–251.

Yang, Y., Shao, M., Kessel, S., Li, Y., Lu, K., Lu, S., Williams, J., Zhang, Y., Zeng, L., Noelscher, A.C., Wu, Y., Wang, X., Zheng, J., 2017. How the OH reactivity affects the ozone production efficiency: case studies in Beijing and Heshan, China. Atmos. Chem. Phys. 17, 7127–7142.

Yee, L.D., Kautzman, K.E., Loza, C.L., Schilling, K.A., Coggon, M.M., Chhabra, P.S., Chan, M.N., Chan, A.W.H., Hersey, S.P., Crounse, J.D., Wennberg, P.O., Flagan, R.C., Seinfeld, J.H., 2013. Secondary organic aerosol formation from biomass burning intermediates: phenol and methoxyphenols. Atmos. Chem. Phys. 13, 8019–8043.

Zhang, X., Lambe, A.T., Upshur, M.A., Brooks, W.A., Be, A.G., Thomson, R.J., Geiger, F.M., Surratt, J.D., Zhang, Z., Gold, A., Graf, S., Cubison, M.J., Groessl, M., Jayne, J.T., Worsnop, D.R., Canagaratna, M.R., 2017. Highly oxygenated multifunctional compounds in α-pinene secondary organic aerosol. Environ. Sci. Technol. 51, 5932–5940.